33rd Annual International Conference of the IEEE EMBS
Boston, Massachusetts USA, August 30 - September 3, 2011

An Image-Based Guidewire Navigation Method for Robot-Assisted Intravascular Interventions

Cheng Ji and Zeng-Guang Hou, Xiao-Liang Xie

***Abstract*— This paper aims at using a newly developed robotic system to automatically deliver guidewires or catheters to the target site on percutaneous coronary interventions (PCIs) or electrophysiology interventions. An autonomous delivery strategy using electromagnetic tracking technology is introduced and phantom experiments are performed to validate this strategy. In order to advance the guidewire into the planned branch, the strategy classifies this branch selection problem into three cases according to the width of the vessels and employs an image-based algorithm for the first and second cases. Another image-based algorithm specifically designed for the third case is also presented.**

***Index Terms*— electromagnetic tracking, cardiology interventions, image-guided navigation**

I. Introduction

We developed a robotic system to assist cardiology surgeons to perform medical procedures. The robot consists of a robotic manipulator, a joystick and a guidewire delivery device. The delivery device mimics the surgeon's action during interventions to control the guidewire for axial and rotational movements. In clinical procedures, surgeons use coronary digital subtraction angiography (DSA) to check guidewire's position in patient and manipulate a joystick to control the delivery device alternately rotating and advancing the guidewire to the target site. A high precision torque sensor is mounted on the delivery device to measure resistance force on the guidewire during interventions. When the measured torque is larger than the predetermined threshold, the system will halt and wait for the clinician to perform corresponding operations. This system also has a navigation unit which merges DSA with preoperative CT image to offer surgeons instinctive visualization. This system has been successfully tested in animal trial as shown in Fig. 1.

Since it is usually difficult for surgeons to determine the spatial relationship between a guidewire and overlapping vessels from intraoperative DSA, we wonder whether this robot could accomplish operations under the assistance of preoperative CT image and intraoperative electromagnetic tracking information instead of surgeons' discernment and supervision. With this system, harmful X-ray is not necessary and surgeons' work will be largely reduced. These are the main advantages of this robot-controlled navigation and delivery system. An experiment to prove the feasibility is proposed and material preparations for the experiments are performed.

This research is supported in part by the National Hi-Tech R&D Program (863) of China (Grant #2010AA044001).

Key Laboratory of Complex Systems and Intelligence Science, Institute of Automation, Chinese Academy of Sciences, Beijing, China cheng.ji@ia.ac.cn, hou@compsys.ia.ac.cn, xiaoliang.xie@ia.ac.cn

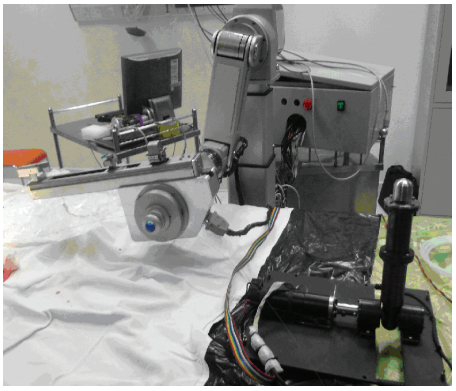

Fig. 1. The cardiology interventions robot was tested in pig PCIs.

First, an original image of human's abdominal aorta is acquired from CT scan devices. After segmentation and volume rendering, we extract the vessel contours and centerlines from the rebuilt CT image as shown in Fig. 2(a). Meanwhile, the radius of the vessel is also computed for each centerline point, and the points where two centerlines meet are regarded as bifurcations. This processed image with contours and centerlines is used for preoperative path planning, diagnosis and intraoperative navigation. Second, we adopt the 3D data to build a precise thermal resin vessel cavitary phantom using rapid prototyping manufacturing (RPM) as shown in Fig. 2(b). Clearly, the target of our experiments is using our newly developed robot system to automatically deliver a guidewire following a preoperative planned path inside thermal resin phantom. Third, in order to track the guidewires or catheters, the Aurora tracking system (NDI, Waterloo, Ontario, Canada) is used, and a tracking guidewire which is bonding Aurora 5 DOF electromagnetic sensor on its tip is also available as shown in Fig. 3. After above three steps, a delivery strategy is proposed to ensure the completion of the experimental target, and an image-based algorithm is adopted in the strategy to ensure the guidewire is driven into correct branch when a bifurcation is encountered. The vessel contours and centerlines we obtained at the first step are utilized in the strategy and the algorithm.

This paper is organized as follows. Section II discusses some issues involved with the experiments and the delivery strategy. The algorithm of branch selection is introduced in section III and the simulation result is given in section IV. Finally, some conclusions are included in section V.

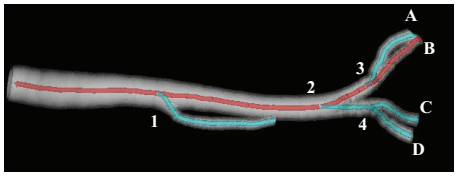

(a)

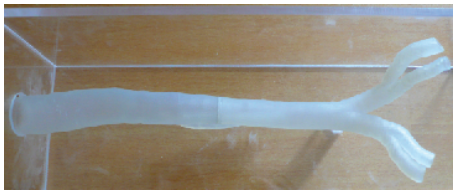

(b)

Fig. 2. (a) The rebuilt CT image of human abdominal aorta; (b) The human abdominal aorta phantom.

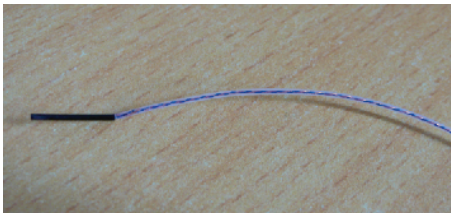

Fig. 3. The Electromagnetic Guidewire.

II. Delivery Strategy

A. Registration

As we already obtained a 3D CT data set of this phantom with contours and centerlines before experimental procedure, an image-to-patient registration is required for the purpose of tracking the guidewire's position during phantom interventions. In recent medical navigation literature, there has been a tremendous amount of work on discussing patient-to-image registration [1] [2] [3] [4]. In our experiments, a two-step registration is performed to produce a homogeneous transformation matrix and the maximal registration error is about 1.3 mm. A simple points registration was firstly adopted to attain a preliminary result and then iterative closet point (ICP) registration was performed to get a better result. The preliminary result from first step will significantly improve ICP's convergence speed. Since the aim of our experiments only focuses on proving the feasibility of advancing the guidewire to target site and the guidewire tip can not be directly controlled, we will not pay too much attention on the approximation precision and thus we reckon the registration error is acceptable. The homogeneous transformation matrix we derived from registration is used to translate guidewire's positions and orientations in NDI magnetic field coordinate to those in image coordinate during experimental interventions.

B. The model of guidewire tip

The tracking guidewire has a flexible tip in which an electromagnetic sensor is mounted. However, the sensor is not located at the apex of the flexible tip but about 3.4 mm away from the apex. Here we propose a simplified model for the tip of tracking guidewire as shown in Fig. 4. As shown in the figure, the tip model consists of a straight line and a curve. The straight line represents the flexible tip and the curve represents the rest section of the guidewire which we call "guidewire body" in the following pages. L_1 (3.4 mm) is the distance from the sensor to the apex of the tip, and L_2 is the distance form the sensor to the end of the tip, about 5.2 mm. The bending angle between the tip and the guidewire body varies from 0 degree to about 60 degree, and in natural state the bending angle keeps about 20 degree. L_0 is the vertical distance from the apex of the tip to guidewire body in natural state, about $(L_1 + L_2)\sin(2\pi(20/360)) = 2.94$ mm.

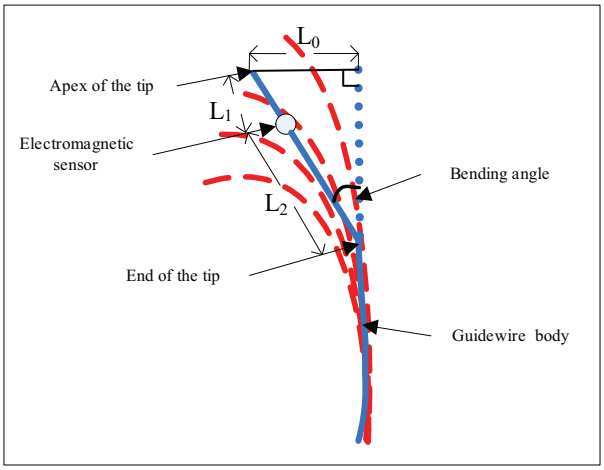

Fig. 4. The model of guidewire tip.

The position and orientation of the guidewire tip can be given by

$$\begin{pmatrix} x_1 \\ y_1 \\ z_1 \\ 0 \end{pmatrix} = T \begin{pmatrix} x_0 \\ y_0 \\ z_0 \\ 0 \end{pmatrix} + TL_1 \begin{pmatrix} D_x \\ D_y \\ D_z \\ 0 \end{pmatrix}$$

$$\begin{pmatrix} x_2 \\ y_2 \\ z_2 \\ 0 \end{pmatrix} = T \begin{pmatrix} x_0 \\ y_0 \\ z_0 \\ 0 \end{pmatrix} - TL_2 \begin{pmatrix} D_x \\ D_y \\ D_z \\ 0 \end{pmatrix}$$

Where $\begin{pmatrix} x_1 & y_1 & z_1 & 0 \end{pmatrix}^T$ and $\begin{pmatrix} x_2 & y_2 & z_2 & 0 \end{pmatrix}^T$ represent the positions of the apex and the end for the tip. And $\begin{pmatrix} x_0 & y_0 & z_0 & 0 \end{pmatrix}^T$ is the tracked electromagnetic sensor position in image space, $\begin{pmatrix} D_x & D_y & D_z & 0 \end{pmatrix}^T$ is the direction unit vector of the sensor's longitudinal axis. T stands for the homogeneous transformation matrix.

C. Phantom paths map

The phantom used in the experiments has nine sections of centerline and four bifurcations (1,2,3,4) as shown in Fig. 2(a). We store these centerlines and bifurcations with vessel contours in database before experiments. The phantom owns one entrance and four exits (A,B,C,D). One of these exits

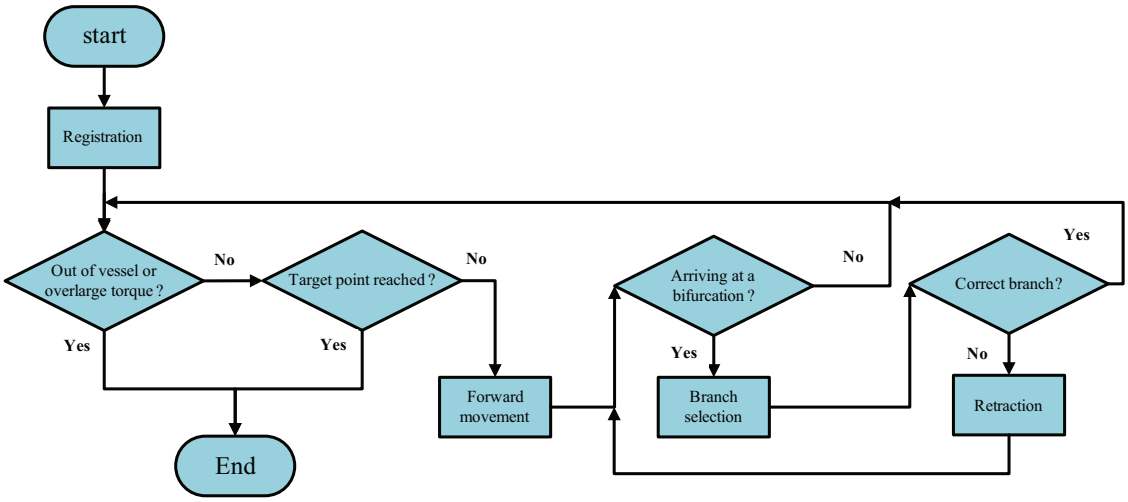

Fig. 5. The architecture of delivery strategy.

is selected as target site and the last point of related branch's centerline is considered as target point. Once the target point is chosen, the delivery path will be automatically planned based on the database. Each planned path consists of four centerlines, and three of four bifurcation will be met during the interventions. It's clear that, the direction from entrance to exits in the phantom experiment is not the actual direction surgeons perform the delivery in clinical practice; however, the opposite direction dose not affect the purpose of our experiments.

D. Delivery strategy

At the beginning of the experiment, we lay the tip of the guidewire in the entrance, then perform an autonomous delivery strategy to control the delivery device to advance the guidewire following planned path to target point. After registration, the position and orientation of the guidewire's tip in CT image coordinate are tracked in real time until the end of experiment. The structure of the strategy is shown in Fig. 5.

The strategy works as follows.

(1) We examine whether the tip is out of the vessel contour or the measured torque is over threshold. In fact, the tip is not able to pass through the vessel in this phantom experiment due to stiff material; however, the torque may be too large when harsh collision occurs. If these situations happen, then the system will halt, otherwise we go on to next step.

(2) The CT image is used to check whether the tip reached the target point. If the distance between the current tip position and the target point in axial direction is smaller than 0.1 mm, we conclude that the target point is reached and the experiment will terminate, otherwise we go on to next step.

(3) We check whether the tip is close to a bifurcation. The bifurcation is a point at where two different centerlines meet, so it is also a centerline point and has a related radius of the vessel we computed before experiment. If the distance between current tip position and the bifurcation is smaller than the radius, we stop the guidewire from forward movement and skip to step 4, otherwise we keep the guidewire for axial movement at a constant predetermined speed and jump back to step 1.

(4) An image-based algorithm is adopted to rotate the guidewire tip to desired orientation and then advance the guidewire for certain distance in order to insert it into the planned branch. Then we go to step 5. The details about the algorithm are introduced in Section III.

(5) In this step, we verify whether the guidewire has been driven into correct branch and away from the bifurcation. If the guidewire is in planned branch and has enough distance away from the bifurcation, the guidewire is considered has crossed the bifurcation and jump to step 1; if the guidewire is in planned branch but not enough far away from the bifurcation, we further move the guidewire for a small distance and jump back to step 5; if the guidewire is not in correct branch, we have to retract the guidewire for the same distance we advanced the guidewire for in step 4 and jump back to step 4.

Following above steps, the workflow will terminate only when target point is reached or overlarge torque on the guidewire is measured. It is noticed that the algorithm we used in step 4 couldn't 100 percent guarantee the guidewire being inserted into planned branch; thus, a detection-retraction mechanism was adopted in step 5 in a higher level.

III. Branch Selection Algorithm

The main difficulty in delivery strategy is how to advance the guidewire to planned branch when the guidewire arrives at a bifurcation. As the orientation of the tip is obtained as feedback in real time, there are complicated situations. For the guidewire usually contacts with vessel wall during intervention, when the delivery device rotates the guidewire a certain angle at the end, the tip of the guidewire dose not always follow the same angle and is distorted erratically.

In order to describe and solve this problem, we classify it into three different cases according to the width of the blood vessels. Methods for quantitative coronary analysis (QCA) indicated in [5] [6] inspire us to design following algorithms.

(1) In the first case, the vessel width is two times bigger than L_0. The algorithm for ordinary first case is shown in Figs. 6,7. In Fig. 6, B is the centerline for the planned branch. The radius of the bifurcation is r and point M on B is r away from the bifurcation. A sphere centers at M and the radius of the sphere is naturally the centerline point M's radius obtained from CT image. When guidewire tip's approaching to the bifurcation is detected, we stop guidewire's constant speed movement and deliver it a certain distance. Fig. 7 indicates how the distance is calculated. Point q is the tip end's present position and point p is the position of guidewire's tip end after certain distance movement. Here, we attain a cone by rotating the guidewire tip around $\overrightarrow{qp}$ and the tone intersects with the sphere at point a and point b. When different distance is delivered, the intersection length from a to b varies. In this way, we calculate the intersection length for every delivery distance by a 0.1 mm length step from present tip end position to the position where the tip is out of the bifurcation sphere, and the distance related with the longest intersection length is regarded as final result. After the guidewire has been delivered for the calculated distance, we further rotate the guidewire for an appropriate angle in order to put the tip apex near the middle point between a and b. After the desired orientation has been reached, the guidewire will be delivered axially again. It is noticed that, in Fig. 7 only present tip end's position is used to determine the cone's axis direction; however, in our practical project, five additional previous tip end's positions with different weights are involved to make the direction more reliable.

The above algorithm derives from the ideal conditions. In experimental practise, the guidewire tip usually is close to vessel walls and the rotation actions for tip may cause collisions and bounces between tip and vessel walls. However, despite collisions and bounces occur, the algorithm also works and the desired orientation is largely reached as shown in Fig. 8(a). In fact, in some cases where the tip orientation complied with desired direction, the rotation is performed only for the purpose of adjusting the position of tip end. For example, in Fig. 8(b), the right branch is the planned branch. Though the direction of tip (the red real line) meets the desired direction, the guidewire will enter into the wrong path if we keep delivering it as the two blue lines indicate, since the guidewire is too close to vessel walls on left side. Accordingly, we first rotate the guidewire for 180 degrees. As a result, the tip bounces apart from the vessel wall, and the tip end moves a distance to right side. Then we rotate another 180 degrees and delivere it forward into the right branch. It is worthy to declare, after the 360 degrees rotation, the tip end's relocation brings certain change of tip's orientation as a disadvantage, a readjustment for tip direction is necessary. We also noticed, sometimes the problem indicated in Fig. 8(b) can not be solved by one time 360 degrees rotation. In these cases, the rotation should be repeated for several times until the tip end's position is acceptable.

How to determine whether the tip end's position is acceptable is as follows: After 360 degrees rotation, we first move the guidewire for 0.2 mm forward movement and several

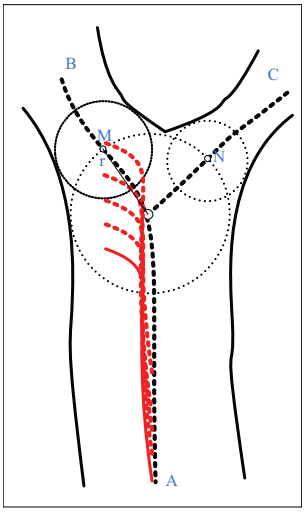

Fig. 6. The first case of branch selection.

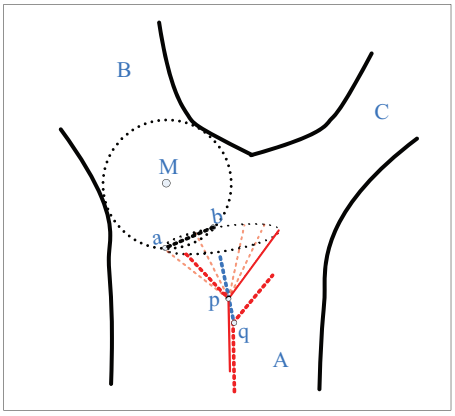

Fig. 7. The algorithm for calculating delivery length and rotation angle in first case.

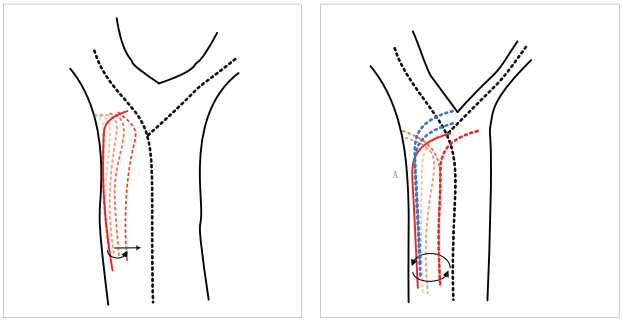

(a) (b)

Fig. 8. (a) The way collisions and bounces between guidewire and vessel wall influence the direction; (b) The method for relocating the tip end in first and second cases.

points in this trail are recorded and used to obtain the axis direction of the cone needed in next step; Then the model given in Fig. 7 is adopted again to calculate whether the cone intersects with the sphere which centers at M. The tip end's position is acceptable when intersection occurs.

(2) In the second case, the diameter of the vessel before the bifurcation is met is between L_0 and $2L_0$. The methods used in second case is similar with those in first case. But noticed, the problem show in Fig. 8(b) is even more common as the vessels are narrower. Accordingly, the method given in Fig. 8(b) is even more effective in this case.

(3) The third case is simpler than the two previous cases. If the vessel width before the bifurcation is met is smaller than L_0, then the tip of the guidewire will be straighter than its natural status, and the bending angle of the tip is less than 20 degree. In this case, the tip of the guidewire is on contact with the vessel wall all the time. Here, the sequence for rotation and axial delivery changes: we first rotate the guidewire tip to a desired direction and then push the guidewire forward as showed in Fig. 9(a). It is noticed that the desired direction is calculated in a cross-section perpendicular to the centerline. The algorithm is presented as in Fig. 9(b). First, we compute the desired direction: P_1 is a plane which is perpendicular to the centerline A at the bifurcation. L is a section from the bifurcation to centerline point M which is in the planned branch B and the length of L is the radius of the bifurcation. Line L' is the projection of L on the plane P_1 and the direction of line L' is the desired direction. Then the guidewire is rotated to L''s direction before the time when the guidewire confronts with the bifurcation. Here, we draw a plane (P_2) which is perpendicular to A and includes present point of tip end. In this way, we rotate guidewire step by step, until the projection of the tip's direction vector on P_2 is largely close to desired direction. After the desired direction is reached, we keep pushing the guidewire to the bifurcation, finally the guidewire tip will enter into the planned branch.

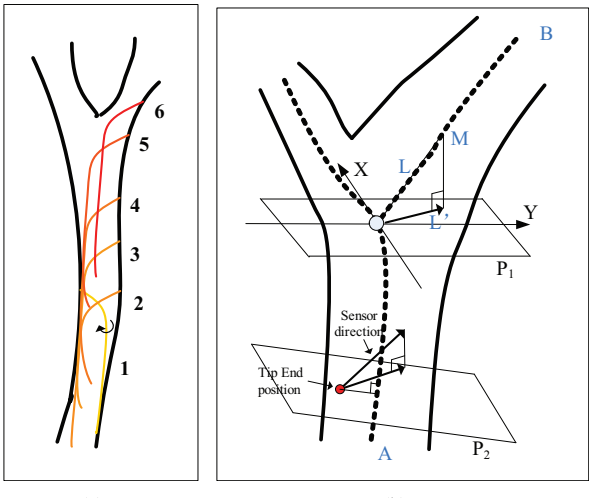

(a) (b)

Fig. 9. (a) The delivery flow in third case: rotation movements from position 1 to position 2, axial movements from position 2 to position 6; (b) The algorithm for desired direction and guidewire tip direction calculated in planes perpendicular to the centerline.

TABLE I

DETAILS OF THE RESULT.

Target site	Bifurcations met on delivery path	Wrong selection at first bifurcation (times)	Wrong selection at second bifurcation (times)	Wrong selection at third bifurcation (times)
exit A	1,2,3	0	1	5
exit B	1,2,3	0	0	0
exit C	1,2,4	0	1	1
exit D	1,2,4	0	1	3

IV. EXPERIMENTAL RESULT

We set the four exits as target sites respectively and perform the interventions 10 times. In each individual procedure 3 bifurcations are met along the path. As 120 bifurcations were met during the entire experiments, incorrect selections took place 12 times. If the guidewire was inserted into the wrong path, we had to retract and deliver it again. Finally, the guidewire reached destinations in all 40 times interventions. We are satisfied with the result, but clearly, there are space to improve the one-time success rate. One result is given in Fig. 10. In this figure, the red line represents the centerline of planned path and a number of short white sections stand for the position and orientation of the guidewire tip. The detail of result is shown in Tab. I. The symbols of bifurcations are indicated in Fig. 2(a).

We also perform manual intervention on the phantom 10 times targeting each exits respectively in order to compare the average intervention time with autonomous delivery, the result is shown in Tab. II. Clearly, the autonomous delivery needs more time than manual delivery, which is partly related to the slow axial speed in autonomous delivery, 25 mm per second. And the autonomous delivery algorithm takes a long time to reach desired orientation during branch selection.

TABLE II

COMPARISON OF THE AVERAGE TIME TAKEN IN AUTONOMOUS DELIVERY AND MANUAL DELIVERY.

Target site	Manual time (seconds)	Autonomous time (seconds)
exit A	4.5	8.6
exit B	2.8	6.7
exit C	3.1	6.9
exit D	4.2	8.3

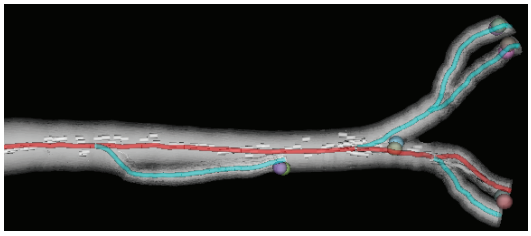

Fig. 10. An experimental result.

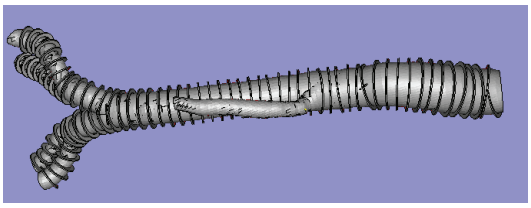

Fig. 11. The STL-format data of the scaled phantom used in rapid prototyping manufacturing.

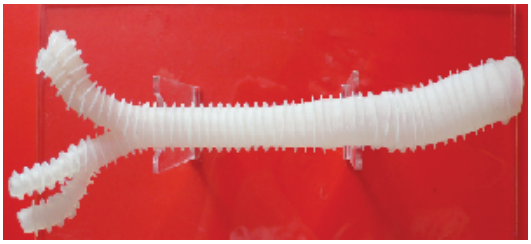

Fig. 12. The phantom with scales.

The accuracy is another important criterion we concern and our initial idea for the measurement of the experimental accuracy is to use the DSA image. However, from an engineering point view, even the DSA scanner system is finely calibrated, it also will bring some errors that might influence the objectivity of the measurement and the image resolution limitation also reduces the precision of the measurement. Therefore we design a new phantom with scales to estimate the final system accuracy. Along the smoothed centerlines, points are chosen every 5 mm and the tangent vectors are calculated. The planes (cross-sections) are completely determined by these centerline points and tangent vectors. And on each cross-section plane, a round, whose radius is 1.5 mm bigger than the corresponding vessel radius, is attached to the original phantom STL-format data to form a protuberant scale, as shown in Fig.11. The scaled phantom produced by rapid prototyping manufacturing is illustrated in Fig.12.

In Fig. 13, the target point is the centerline point on the round scale which is marked by the blue line and the distance between the guidewire tip and the target cross-section in axial direction is in a range from 1 to 2 mm. We perform the experiment 10 times for each exits respectively, and the maximum visual distance between the tip and the target cross-section is smaller than 2 mm. According to the suggestion given by the collaborating experienced surgeons and other studies on cardiac navigation in [2] [7] [8], 3 mm is a proper error requirement for cardiac intervention navigation and our system accuracy meets this requirement. It is noticed that, considering our intended application and the flexibility of the guidewire tip, it is more reasonable to measure the accuracy in axial direction than in spatial distance.

V. Conclusion

In this paper, we proposed an autonomous delivery system for robot-assisted PCIs. Phantom experiments were performed to verify the feasibility of the system. NDI electromagnetic tracking system and tracking guidewire were used in this experiment. First, patient-to-image registration, guidewire tip model and phantom model were introduced, and then a delivery strategy was presented for delivering the guidewire to target site. In order to advance the guidewire into the planned branch, we devised two image-based algorithms for three cases classified by the width of the vessel. We also discussed several detailed problems in the first case and offered related resolvent. In the end, the visual accuracy results derived from phantom experiments with scales confirmed the conclusion that the autonomous delivery system was viable.

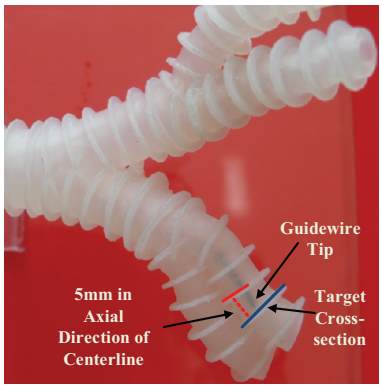

Fig. 13. The measurement of the autonomous delivery accuracy in phantom with scales.

References

[1] P. Woerdeman, P. Willems, H. Noordmans, C. Tulleken, and J. van der Sprenkel, "Application accuracy in frameless image-guided neurosurgery: a comparison study of three patient-to-image registration methods," *Journal of Neurosurgery: Pediatrics*, vol. 106, no. 6, 2007.

[2] W. Birkfellner, F. Watzinger, F. Wanschitz, R. Ewers, and H. Bergmann, "Calibration of tracking systems in a surgical environment," *IEEE Transactions on Medical Imaging*, vol. 17, no. 5, pp. 737–742, 2002.

[3] K. Finnis, Y. Starreveld, A. Parrent, A. Sadikot, and T. Peters, "Three-dimensional database of subcortical electrophysiology for image-guided stereotactic functional neurosurgery," *IEEE Transactions on Medical Imaging*, vol. 22, no. 1, pp. 93–104, 2003.

[4] G. Eggers and R. Marmulla, "Template-based registration for image-guided maxillofacial surgery," *Journal of Oral and Maxillofacial Surgery*, vol. 63, no. 9, pp. 1330–1336, 2005.

[5] S. Ramcharitar, Y. Onuma, J. Aben, C. Consten, B. Weijers, M. Morel, and P. Serruys, "A novel dedicated quantitative coronary analysis methodology for bifurcation lesions." *EuroIntervention: journal of EuroPCR in collaboration with the Working Group on Interventional Cardiology of the European Society of Cardiology*, vol. 3, no. 5, p. 553, 2008.

[6] C. Girasis, J. Schuurbiers, Y. Onuma, J. Aben, B. Weijers, E. Boersma, J. Wentzel, and P. Serruys, "Two-dimensional quantitative coronary angiographic models for bifurcation segmental analysis: In vitro validation of caas against precision manufactured plexiglas phantoms," *Catheterization and Cardiovascular Interventions*.

[7] D. Cho, C. Linte, E. Chen, C. Wedlake, J. Moore, J. Barron, R. Patel, and T. Peters, "Predicting Target Vessel Location for Improved Planning of Robot-Assisted CABG Procedures," *Medical Image Computing and Computer-Assisted Intervention–MICCAI 2010*, pp. 205–212, 2010.

[8] C. Linte, M. Wierzbicki, J. Moore, S. Little, G. Guiraudon, and T. Peters, "Towards subject-specific models of the dynamic heart for image-guided mitral valve surgery," in *Proceedings of the 10th international conference on Medical image computing and computer-assisted intervention*. Springer-Verlag, 2007, pp. 94–101.